Comparative optical reflectance study of the superconducting KHg-graphite and $CsBi_x$-graphite intercalation compounds

M. H. Yang, P. A. Charron, R. E. Heinz, and P. C. Eklund
Department of Physics and Astronomy, University of Kentucky, Lexington, Kentucky 40506
(Received 1 June 1987)

We report the results of a comparative optical reflectance study at room temperature of the stage-1 and stage-2 $CsBi_x$ and KHg graphite intercalation compounds (GIC's) in the energy range 0.2–10 eV. A Kramers-Kronig analysis is carried out to determine the dielectric function $\epsilon(\omega)=\epsilon_1(\omega)+\epsilon_2(\omega)$ and the intra- and interband contributions to $\epsilon(\omega)$ are identified. The dielectric function for the respective compounds are analyzed in terms of a schematic density-of-states model involving contributions from two-dimensional graphite π band(s) and intercalate bands. Separate contributions from the π and intercalate electrons to the free-carrier plasma frequency are determined via the identification of the carbon $\pi\rightarrow\pi^*$ interband absorption threshold $E_T\sim 2E_F$, where E_F is the Fermi energy measured with respect to the approximate mirror plane in the carbon π-band structure. The analysis of the optical data indicates that for $CsBi_x$ GIC's, the electrical transport properties should be dominated by the light carbon π-band electrons in contrast to the KHg GIC's, where the analysis indicates the transport properties should strongly depend on free carriers in both the π^* and the intercalate band(s). In the case of KHg GIC's, our interpretation of the experimental results are consistent with significant occupation of electronic states with Hg(6*s*) character. Our results suggest that nature of the superconductivity in the KHg and $CsBi_x$ GIC's should be quite different.

I. INTRODUCTION

In this paper, we report the results of optical reflectance studies of the stage $n=1$ and 2 ternary graphite intercalation compounds (GIC's): $CsBi_x$ and KHg GIC's, where the stage index refers to the number of carbon layers which separate the periodically inserted intercalate layers.[1,2] A considerable number of similar optical studies have been carried out on various GIC's over the last ten years, and this work has been reviewed recently for acceptor[3] and donor[4] GIC's. The term acceptor and donor refers, respectively, to whether the intercalate layers are negatively or positively charged. For charge neutrality this charge is balanced by opposite-sign charge residing primarily on the carbon layers adjacent to the intercalate layers.[1,2] The experimental data for $CsBi_x$ GIC's presented here are new and will be compared to data of KHg GIC's which we have reported previously.[5] The optical data for both of these ternary donor GIC systems will be discussed in terms of a two-carrier model developed recently for the potassium hydride ternary GIC by Doll *et al.*[6]

The intercalate layer in stage-1 $CsBi_x$ and KHg GIC's has been studied by diffraction techniques, and found to be composed of a three-layer sandwich *M-X-M*,[7-11] where the two outer alkali-metal layers (*M*) are next to the bounding carbon layers, and the $X=$Bi (or Hg) layer is located very near the center of the intercalate-layer sandwich. The stage-1 α and β phases of $CsBi_x$ GIC's have been shown recently via (001) x-ray diffraction to nearly correspond to the "ideal" or nominal stoichiometries $CsBi_{0.5}C_4$ and $CsBi_{1.0}C_4$ (i.e., the two phases differ by a factor of 2 in the [Cs]/[Bi] ratio and the [Cs]/[C] ratio is $-\frac{1}{4}$ for both phases).[10] Similar to the $CsBi_x$ GIC's, two phases have also been reported for the stage-1 KHg GICs,[8] which on the basis of neutron diffraction have been reported to exhibit a different [K]/[Hg] ratio: 1:1 for the majority phase ($KHgC_4$) and 1:1.3 for the minority phase ($KHg_{1.3}C_4$).

$CsBi_x$ and KHg GIC's have both been reported to superconduct with the following values for the critical temperature T_c: (1) $CsBi_x$ GIC's (Ref. 9)—$T_c\approx 4.0$ K (stage 1, α phase), $T_c\approx 2.4$ K (stage 1, β phase), and $T_c\approx 2.8$ K (stage 2, β phase), and (2) KHg GIC's (Refs. 11 and 12)—$T_c\approx 0.73$ K ($KHgC_4$) and $T_c\approx 1.96$ K ($KHgC_8$). However, we have measured the ac magnetic susceptibility for several stage -1 α- and β-phase and stage-2 β-phase CsBi GIC samples from different sample preparations, and find no evidence for superconductivity for temperature $T\geq 1.5$ K and pressure $P\leq 7.0$ kbar.[13] The I_c values of these samples agreed to ± 0.02 Å with those reported by Lagrange *et al.*[9]

Unlike the more recently discovered $CsBi_x$ GIC system, the KHg GIC's have been extensively studied during the past several years.[11,12,14-23] To understand the observation that $T_c(KHgC_4$, stage 1$)<T_C(KHgC_8$, stage 2), much effort has been expended[18-21] to determine the electronic structure near the Fermi surface, including the layer charge distribution in the carbon layer and intercalate layers,[18-21] and the density of states at the Fermi level.[22,23] X-ray photoelectron spectroscopy (XPS) (Ref. 18) and electron energy-loss spectroscopy (EELS)[19] of stage-1 and -2 KHg GIC's report that the K(4*s*) states are empty, and that there is more charge in the Hg-derived states for stage-2 $KHgC_8$ than stage-1 $KHgC_4$. Optical interband absorption associated with intercalate

states was observed in reflectance[5,20-21] and electron energy-loss spectroscopy (EELS).[19] A two-dimensional rigid-band calculation[22] and specific-heat measurements[23] of $KHgC_8$ suggest that a large portion of the density of states (DOS) at the Fermi level is from intercalate states. This implies that the electrons in those states play an important role in the transport properties. Similar calculations and measurements in $CsBi_x$ GIC's have not been carried out to date.

In this paper, we report the results of optical studies in the range 0.2–10 eV for $CsBi_x$ GIC's and 0.2–6 eV for KHg GIC's. The dielectric function $\epsilon(\omega)=\epsilon_1(\omega)+i\epsilon_2(\omega)$ is obtained from a Kramers-Kronig (KK) analysis[24] of the reflectance data, and the intraband and interband contributions to the $\epsilon(\omega)$ are separated by fitting the low-energy data to a Drude free-carrier model. Via the identification of the position of the $\pi\rightarrow\pi^*$ interband threshold energy we obtain an experimental measure of the Fermi energy E_F in the π^* conduction band(s). We use this value in conjunction with an experimental value for the plasma frequency to determine the charge transfer between intercalate and carbon layers. Significant differences emerge from our results for the intercalate-state contributions to the electrical transport properties of $CsBi_x$ and KHg GIC's.

II. EXPERIMENTAL DETAILS

A. Sample preparation and characterization

Lagrange *et al.*[9] first reported the synthesis and superconductivity of the MBi_x-graphite intercalation compounds (M = K, Rb, Cs). However, they did not provide the details of their sample preparation. Our samples were also prepared from plates of highly oriented pyrolytic graphite (HOPG) ($5\times5\times0.3$ mm^3) which were placed in direct contact with molten binary alloy $CsBi_x$ in a sealed tube. They did not report the [Cs]/[Bi] ratio of the initial reacting alloy; we find this ratio is important in determining the phase (α or β) of the resulting material.

$CsBi_x$ alloys were prepared by mixing bismuth shot and slightly warmed liquid cesium metal in a glass beaker inside a He glove box (Vacuum Atmosphere, Inc.) containing a balance ($\sim$10-μg sensitivity) with P_{O_2} and $P_{H_2O}\approx1$ ppm. A powderlike mixture was obtained whose color depends on x. To ensure a homogeneous alloy, we transferred the mixture in the glove box to a stainless-steel tube, sealed by a metal-to-metal compression fitting (Swagelock), and reacted the alloy at a temperature $T\approx600$ °C for 1 d. The resulting alloy (in excess) was then transferred in the glove box to another similar stainless-steel tube containing the HOPG. The intercalation reaction was carried out for temperatures in the range $T\approx600$–700 °C for at least 2 d. Stage-1 α- and β-phase $CsBi_x$ GIC's were obtained at temperatures of $T\approx600$–625 °C using the alloy $CsBi_{0.55}$ and $CsBi_{1.0}$, respectively. Interestingly enough, the stage-2 β-phase $CsBi_x$ GIC was obtained at temperature $T\approx700$ °C using the Bi-poor alloy $CsBi_{0.55}$. Previous x-ray and weight-uptake measurements of the stage-1 α- and β-phase $CsBi_x$ GIC's both supported the finding that the [Cs]/[Bi] ratio in the α and β phases were $\sim$2:1 and $\sim$1:1, respectively. Unfortunately, similar weight-uptake measurement and structure-factor analysis of the (001) x ray were not carried out for the stage-2 β-phase $CsBi_x$ GIC. The intercalate-layer thickness d (Refs. 9 and 10) for the stage-1 and -2 β-phase samples were found from I_c values to be 8.14 and 8.15 Å, respectively, as compared to 7.3 Å for the stage-1 α-phase sample. The similarity in d values for the stage-1 and -2 *β-phase* samples does suggest, however, that the [Cs]/[Bi] ratios are similar, even though they were prepared from 1:1 and 1:0.55 Cs:Bi alloys, respectively.

Samples of KHg GIC's were also prepared from HOPG plates by a method well documented by Lagrange and co-workers in the literature,[7] who reported a nominal stage-1 stoichiometry of $KHgC_4$ for a compound with $I_c=10.24$ Å—this is referred to as the majority phase in Ref. 8. The majority phase is prepared by reacting HOPG with excess HgK alloy (i.e., [K]/[Hg]=1) in a quartz tube at temperature $T\approx350$ °C for several days. The stage-1 minority-phase structure has always been found to coexist with the majority phase[8] and exhibits an $I_c=10.84$ Å. The stage-2 samples were prepared by a two-step process[7] involving the initial preparation of KC_8, and the subsequent reaction of KC_8 with excess Hg to form the stage-2 ternary with nominal stoichiometry $KHgC_8$ ($I_c=13.35$ Å).

Pure-phase, pure-stage [i.e., no impurity-phase (001) x-ray-diffraction peaks greater than $\sim$5% of the largest peak of the majority phase observed] samples were studied optically in this work. The samples were also characterized by Raman scattering, and low-temperature magnetic susceptibility. The latter measurements were used to determine T_c. The values of I_c and T_c (Ref. 16) for the stage-1 (majority phase) and stage-2 KHg-GIC's were found to be in good agreement with the literature.[11,12] However, all the samples of stage-1 (α,β) and stage-2 (β) $CsBi_x$ GIC's studied here (two samples each phase from different batches) did not show any trace of a superconductivity for temperature $T\geq1.5$ K and pressure $P\leq7.0$ kbar, although their I_c values were in good agreement (±0.02Å) with those reported[9] previously. Furthermore, the Raman-active graphitic intralayer phonons of $CsBi_x$ GIC's were found to exhibit a relatively large α,β phase-dependent change in Raman frequencies: 1600 (stage 1 ,α phase), 1595 (stage 1, β phase), and 1604 cm^{-1} (stage 2, β phase).[13]

B. Optical reflectance

The reflectance spectra were taken at near-normal incidence on cleaved c faces. The electric field vector **E** is therefore parallel to the basal plane, and the reflectance probes the basal-plane contribution to the dielectric tensor. The data were collected in two instruments: (1) a prism spectrometer (Perkin Elmer No. 83) using CaF_2 (0.2–2.5 eV) and Quartz (1–6 eV) prisms, and (2) a Seya-Namioka toroidal-grating vacuum instrument (McPherson, No. 225) (6–10 eV). For $\omega<6$ eV the

$CsBi_x$ GIC samples were cleaved in a He glove box and transferred there to a sealed optical cell with a CaF_2 window. $CsBi_x$ GIC's, however, are air stable.[8,9] For measurement in the vacuum spectrometer the $CsBi_x$-graphite samples were momentarily exposed to air to load them into the vacuum sample chamber where they were measured at 10^{-5} torr. Graphite-KHg is not air stable, and these samples were transferred in the He glove box to rectangular glass optical cells equipped with CaF_2 windows attached with epoxy glue (Torr Seal, Varian Associates). The glass cells were subsequently evacuated and tipped off with a torch. The air stability of $CsBi_x$ GIC's is quite remarkable, and the spectra in the (0.2–10)-eV region were found to be insensitive to a limited amount of air exposure (i.e., ~1 d). Further details of the reflectance techniques used in this study are available in Ref. 25.

III. RESULTS

In Fig. 1, we plot the optical reflectance spectra (dots) of the stage-1 α- and β-phase and stage-2 β-phase $CsBi_x$ GIC's, and stage-1 majority phase and stage-2 KHG GIC's in the energy range 0–10 eV. In the region 1–2 eV, each spectrum exhibits a sharp Drude edge (where the reflectance R drops rapidly), characteristic of a metal. The solid lines represent calculated Drude edges in good agreement with the data. For each compound the misfit near the Drude-edge minimum in R is due to strong interband absorption not included in the fit. The broad peak near 5.0 eV observed in all cases is analogous to the ~5.0 eV peak in pristine graphite, which has been identified previously with the peak in the joint density of states (JDOS) associated with the M point.[25,26] The dashed-dotted lines in the figure beyond ~5.5 eV are the uv data extensions.

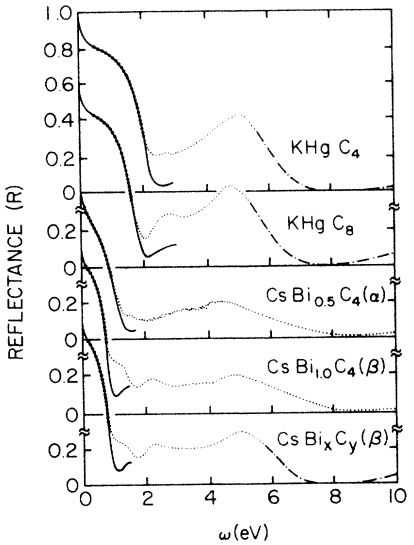

FIG. 1. Room-temperature c face near-normal-incidence reflectance data for the stage-1 and -2 $CsBi_x$ and KHg GIC's. The dotted, dashed-dotted, and solid lines refer, respectively, to the data, high-energy data extension (density-scaled graphite), and calculated free-carrier response (Drude model).

The dielectric functions for the spectra shown in Fig. 1 are calculated from Kramers-Kronig analyses, and are shown in Figs. (2a) and (2b). In order to calculate the phase-shift integral,[24] the data were first extended to lower and higher energy, respectively, as a Drude model and as density-scaled graphite.[4,26] A detailed discussion of this procedure is given in Ref 4. Above ~0.5 eV our results for $R, \epsilon_1, \epsilon_2$ for stage-1,2 graphite KHg are in good agreement with previous work by Preil *et al.*[19] and Heinz *et al.*[5] Below ~0.5 eV we do not observe the weak periodic structure reported previously,[5] and we attribute this prior observation to a spurious interference effect.

The dielectric function $\epsilon(\omega)$ is separated into intraband $\epsilon_{\text{free}}(\omega)$ and interband $\epsilon_{\text{inter}}(\omega)$ contributions by fitting $\epsilon_1(\omega)$, $\epsilon_2(\omega)$, $1/\omega\epsilon_2(\omega)$, and $R(\omega)$ at photon energies well below the interband absorption threshold to a free-carrier contribution given in the Drude approxima-

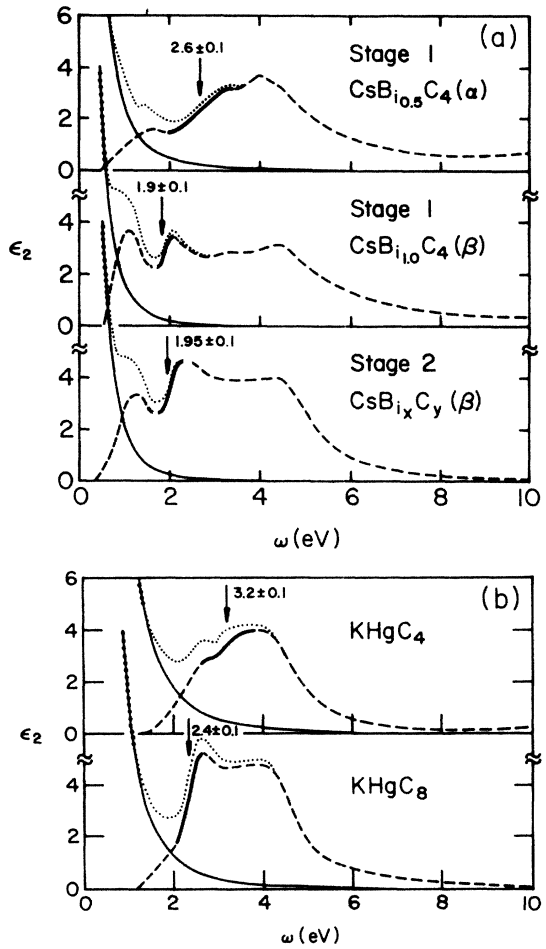

FIG. 2. Imaginary part of dielectric function (dotted lines) of the stage-1 and -2 (a) $CsBi_x$ and (b) KHg GIC's obtained from a Kramers-Kronig analysis of the reflectance data. The free-electron contribution (solid line) and interband absorption contribution (dashed line) are also indicated. The broadened carbon $\pi \rightarrow \pi^*$ interband absorption threshold of each compound is designated by a heavy solid line, and the corresponding arrow indicates the energy value at the midpoint ($\sim 2E_F$) identified with the threshold.

tion by[24]

$$\epsilon_{\text{free}}(\omega)=\epsilon_\infty-\frac{\omega_p^2}{\omega(\omega+i/\tau)}\ , \tag{1}$$

where ϵ_∞ is the core dielectric constant, ω_P is the effective plasma frequency, and τ is the effective carrier lifetime. The solid lines in both Figs. 1 and 2(a) and 2(b) are based on this Drude analysis of the low-energy data. The Drude behavior of the data (dots) is also demonstrated in Fig. 3, where we plot $1/\omega\epsilon_2$ versus ω^2, which is linear for a free-carrier response (solid line) governed by Eq. (1). The departure from the linearity at high energy signals the onset of interband absorption. The values for ω_p, τ, and ϵ_∞ which correspond to the solid lines in Fig. 1–3 appear in Table I.

Referring back to Figs. 2(a) and 2(b), the interband contribution $\epsilon_{\text{inter},2}=\epsilon_2-\epsilon_{\text{free},2}$ is shown for each compound as the dashed line. The onset of the interband absorption is found near 0.5 eV for all three $CsBi_x$-graphite compounds [Fig. 2(a)]. For stage-1 and -2 KHg GIC's [Fig. 2(b)], the onset of interband absorption is found at higher energy near 1.0 eV. We identify a second higher-energy threshold in all compounds (indicated by heavy lines in the figure) with the carbon $\pi\rightarrow\pi^*$ interband absorption threshold. The midpoint of this $\pi\rightarrow\pi^*$ threshold is indicated by the respective arrow, and the positions with estimated error ±0.1 eV are found to be 2.6 (stage 1, α), 1.9 (stage 1, β), and 1.8 eV

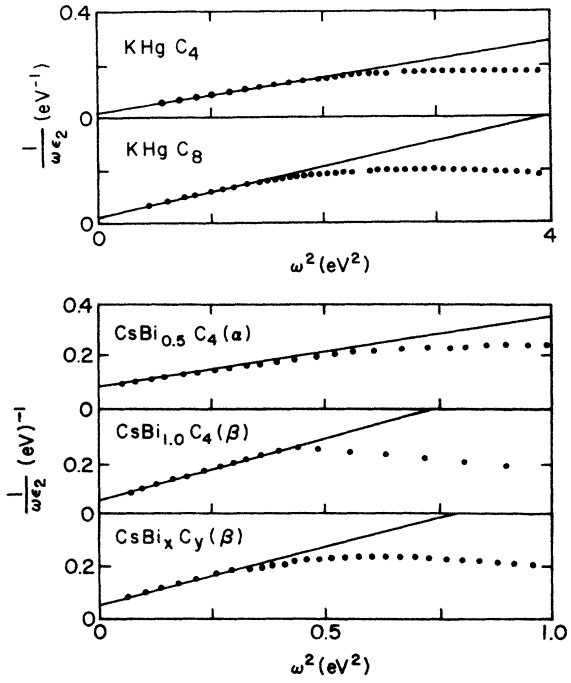

FIG. 3. Plot of $1/\omega\epsilon_2$ vs ω^2 for the stage-1 and -2 $CsBi_x$ and KHg GIC's. Dots are the experimental data and the solid lines are calculated from the Drude parameters which appear in Table I(a). The separation of the curves at higher energy is due to the interband absorption.

TABLE I. Parameters for the (a) stage-1 and (b) stage-2 $CsBi_x$ and KHg GIC's. The values in parentheses represent the estimated error to the right of the decimal point.

(a) Stage 1

Compound Stoichiometry	I_C (Å)	n	Drude parameters ω_p (eV)	$\omega_p\tau$	ϵ_∞
$CsBi_{0.5}C_4$ (α)	10.65 (02)	1	2.6 (05)	5.8	4.8 (2)
$CsBi_{1.0}C_4$ (β)	11.49 (02)	1	2.5 (05)	7.8	8.0 (3)
$CsBi_xC_y$ (β)[a]	14.85 (02)	2	2.6 (05)	8.0	8.0 (3)
$KHgC_4$	10.24 (02)	1	5.1 (1)	9.0	5.1 (2)
$KHgC_8$	13.35 (02)	2	4.7 (1)	10.0	6.3 (3)

(b) Stage 2

Compound Stoichiometry	$\omega_{p,\pi}$ (eV)	$\omega_{p,I}$ (eV)	E_F (eV)	$E_{T,\pi}$ (eV)	$E_{T,I}$ (eV)	Experimental band parameters f_C ($\times10^{+2}$)	f_I	$m_{\text{opt},\pi}$ (m_e)	$m_{\text{opt},I}$ (m_e)
$CsBi_{0.5}C_4$ (α)	2.64 (05)	$\leq$0.23	1.3 (05)	2.6 (1)	0.5	4.0 (4)	$\leq$0.01	0.26 (03)	1[b]
$CsBi_{1.0}C_4$ (β)	2.20 (02)	1.2 (8)	0.95 (05)	1.9 (1)	0.5	2.0 (2)	0.11 (02)	0.19 (01)	1[b]
$CsBi_xC_y$ (α)[a]	2.6 (1)	$\leq$0.23	0.98 (05)	1.95 (10)	0.5	2.0 (2)	$\leq$0.03	0.2 (01)	1[b]
$KHgC_4$	3.0 (05)	4.12 (03)	1.6 (05)	3.2 (1)	1.2	6.0 (7)	1.78 (03)[c]	0.32 (02)	1.35 (05)
							2.8 (03)[d]		2.1 (1)
$KHgC_8$	3.2 (1)	3.48 (00)	1.2 (05)	2.4 (1)	1.1	3.0 (3)	1.75 (02)[c]	0.24 (01)	0.71 (05)
							2.75 (02)[d]		1.1 (1)

[a] For the stage 2 β-phase $CsBi_x$-GIC, the I_c value suggests $x=1.0$ and $y=8$; see text.
[b] Assumed value; see text.
[c] Based on 2 electrons/KHg formula unit; see text.
[d] Based on 3 electrons/KHg formula unit; see text.

(stage 2, β) for the $CsBi_x$ GIC's and 3.2 (stage 1) and 3.0 eV (stage 2) for the KHg GIC's.

IV. DISCUSSION

A. Two-carrier model

The free-carrier contributions to the reflectance spectra of the ternary hydride GIC's KH_xC_4 (stage 1) and KH_xC_8 (stage 2) have been previously analyzed in terms of a two-carrier model,[6] in which the graphitic π electrons at the K point in a graphitic Brillouin zone are described by rigid two-dimensional (2D) bands; carriers in intercalate-derived states were assumed to exhibit an isotropic, energy-independent in-plane effective mass $m_{\rm opt}$ in the range $1 \le m_{\rm opt} \le 2m_e$, where m_e is the free-electron mass. Hybridization of carbon π states with intercalate states is neglected in this model. This two-carrier analysis[6] resulted in three key points regarding the ternary hydride GIC's: (1) the K(4s) states are empty, (2) the hydrogen is chemisorbed, meaning the H(1s) states fall below E_F which therefore fill to make H^- species, and (3) E_F is lowered in the carbon π band to provide the needed electrons for the formation of H^-. We show below that the two-carrier model can also be applied successfully to the $CsBi_x$ and KHg GIC's.

The effective plasma frequency ω_p can be shown to describe well the net contribution to Eq. (1) from two sets of carriers if the lifetime τ_j of the electrons (or holes) in each set ($j=1,2$) satisfies the relation $\omega_{p,j}\tau_j \gg 1$, where $\omega_{p,j}$ is the individual plasma frequency. The square of the effective plasma frequency can then be written as the sum of the squares of the individual plasma frequencies,

$$\omega_p^2 = \omega_{p,\pi}^2 + \omega_{p,i}^2 , \tag{2}$$

where $\omega_{p,\pi}$ and $\omega_{p,i}$ are the specific frequencies appropriate to GIC's here, representing the carbon π-band conduction electrons and the free electrons in intercalate-derived states, respectively.

We use the 2D tight-binding model of Blinowski and Rigaux (BR) (Ref. 27) to describe approximately the graphitic π bands. The K-point expansion of their results leads to simple analytical expressions for the Fermi energy E_F (Ref. 27) and optical mass $m_{\rm opt}$ (Ref. 25) given by

$$E_F = \gamma_0(\pi/\sqrt{3}f_C)^{1/2}, \quad \text{stage 1,2} \tag{3}$$

$$m_{\rm opt} = \frac{4}{9}\frac{\hbar^2 E_F}{\gamma_0^2 b^2}, \quad \text{stage 1} \tag{4}$$

$$m_{\rm opt} = \frac{4}{9}\frac{\hbar^2 E_F}{\gamma_0^2 b^2}\frac{E_F^2-\gamma_1^2/4}{E_F^2-\gamma_1^2/2}, \quad \text{stage 2} \tag{5}$$

where γ_0 and γ_1 are the in-plane and c-axis nearest-neighbor transfer integrals, respectively, b is the in-plane C—C bond length, and f_C is the carbon π-band charge density in units of electrons per C atom. It should be noted that a factor-of-2 error appears in the relationship between E_F and f_C for stage 2 in Ref. 27. In the present work, γ_0 and γ_1 are chosen to be 2.9 and 0.37 eV, which are typical of values commonly used in the literature.[6,25,28] If we designate the density of free carriers in the intercalate bands as f_I (in units of electrons per intercalate formula unit), we obtain from the standard definition of the plasma frequency[24] an expression for the effective plasma frequency given by

$$\omega_p^2 = \frac{4\pi e^2 f_C}{\Omega_C m_{{\rm opt},\pi}} + \frac{4\pi e^2 f_I}{\Omega_I m_{{\rm opt},I}} , \tag{6}$$

where Ω_C and Ω_I are, respectively, the volume per C and I unit (i.e., I = KHg or $CsBi_x$) in the GIC. The first term in Eq. (6) is the 2D π-electron contribution, and the second term is the contribution from the 3D intercalate-derived states which is parametrized by the isotropic optical mass $m_{{\rm opt},I}$.

The threshold for the carbon $\pi \rightarrow \pi^*$ absorption involves transitions to final states at E_F in the π^* band.[3,4,27] If the approximate mirror symmetry in the π-band structure is preserved to a large extent after intercalation, the inter-π-band absorption threshold $E_{T,\pi}$ is given by $E_{T,\pi} \approx 2E_F$,[3,4,27] where E_F is measured relative to the mirror plane in the π-band structure. Thus the identification of the $\pi \rightarrow \pi^*$ threshold [indicated by arrows which locate the midpoint of the broadened structure in Figs. 2(a) and 2(b)] is an important experimental measure of the Fermi-level position in the carbon π bands.

B. $CsBi_x$ GIC's

CsC_8 can be viewed as the Bi-free binary related to $CsBi_x$-graphite. The Drude edge in the reflectance spectrum of this binary compound is located at ~ 2.3 eV.[29,30] Unfortunately, the CsC_8 reflectance data[29,30] have not been as extensively analyzed as other binary GIC's (Refs. 3, 4, 20, and 21). Upon the addition of Bi to the Cs GIC the position of the Drude edge down shifts by ~ 1.3 eV, to a value of ~ 1.0 eV in the stage-1,2 ternary $CsBi_x$-graphite compounds. Such a downshift is consistent with a transfer of light π-band electrons to Bi states with heavier electronic mass. This transfer can be addressed quantitatively within the framework of the two-carrier model.

Let us first consider the case of the stage-1 α-phase $CsBi_x$ GIC, and assume for the moment that the dominant *free-carrier* contribution to the dielectric function $\epsilon(\omega)$ originates in the carbon π-electron term [Eq. (2)]; i.e., we take the experimental value of ω_p (stage -1 α phase) $= 2.6$ eV $= \omega_{p,\pi}$. Using the BR model we calculate E_F from $\omega_{p,\pi}$ and find $E_F = 1.22$ eV, and therefore $E_{T,\pi} \approx 2E_F = 2.45$ eV, in close agreement with the estimated position of the midpoint of $\pi \rightarrow \pi^*$ interband absorption structure in $\epsilon_2(\omega)$ at 2.6 eV in Fig. 2(a). Similar reasoning applied to the stage-1 β phase and stage-2 β phase $CsBi_x$ GIC's leads to predictions for inter-π-band thresholds also in close agreement with the observed position of respective midpoint of inter-π-band threshold. Thus we identify all these higher-energy interband threshold structures with the $\pi \rightarrow \pi^*$ threshold. The $\pi \rightarrow \pi^*$ threshold has been shown recently by Shung[31] to broaden about $2E_F$ due to electron-electron scattering. We therefore use the midpoint (uncertain to about ± 0.1

eV) of this interband threshold structure as the experimental value for $2E_F$ measured relative to the approximate mirror plane in the carbon π band(s).[27] These values of E_F can in turn be used in Eqs. (3)–(5) to obtain experimental values for $\omega_{p,\pi}$, f_C, and $m_{\text{opt},\pi}$. The values for these π^*-band parameters are displayed in Table I. We note that the optical mass of the π electrons is found to be $\sim 0.2m_e$, which ensures that the π electrons will dominate the intraband contribution.

We next turn our attention to lower-energy interband structure in the $CsBi_x$ GIC data. Photoemission studies[32,33] on the semiconducting $CsBi_{0.33}$ alloy indicates that there are two low-lying occupied Bi($6p$) valence bands separated by a spin-orbit splitting of $\sim 1-2$ eV. These bands are separated by a semiconducting gap (~ 0.7 eV) from a higher-lying conduction band. The experimental $CsBi_{0.33}$ density of states (DOS) (Ref. 33) is shown in the inset to Fig. 4. In view of the DOS reported for $CsBi_{0.33}$, it is compelling at this time to also identify the onset of low-energy interband absorption near ~ 0.5 eV in the three $CsBi_x$ GIC's with transitions across a gap in the $CsBi_x$ contribution to the DOS of the GIC's. In this spirit we propose the following schematic DOS model for the $CsBi_x$-GIC to qualitatively understand the optical data. This model is shown in Fig. 4. The solid and dashed dotted lines refer, respectively, to π- and intercalate-derived contributions to the total DOS. The Fermi level E_F is seen to cut through the π^* band and the top of the Bi($6p$) band. We view the upper Bi($6p$) band as taking a large fraction of the Cs($6s$) electrons which would otherwise be transferred to the carbon π^* band (as in the case of the binary CsC_8), thereby lowering the Fermi level E_F in the π^* band relative to its position in the Bi-free compound. Because the experimental value of the effective plasma frequency ω_p [Eq. (2)] in all three $CsBi_x$ GIC's is very nearly the same as $\omega_{p,\pi}$, the small difference between ω_p and $\omega_{p,\pi}$ is provided in our model by holes in the Bi($6p$) band. The number of Bi($6p$) holes (or their upper bound) can be calculated from Eq. (6) if we estimate the optical mass of the holes to be $\sim 1m_e$. We therefore find f_I (i.e., the number of holes per $CsBi_x$ unit) to be ≤ 0.01 (stage- 1 α phase), 0.11 ± 0.02 (stage 1 β phase), and ≤ 0.03 (stage 2 β phase), respectively. It is interesting to observe that the stage-1 α phase (Bi-poor) compound has a smaller value of f_I than the β phase (Bi-rich) compound. This seems to suggest that the larger the value of f_I, the larger the [Bi]/[Cs] ratio. However, we further note that the value of f_I obtained for the stage-2 β phase compound is nearly the same as the value obtained for the stage-1 α-phase one. Thus we can draw no simple conclusions from a rigid-band interpretation of these results. We believe it is likely that the value of f_I depends not only on the [Bi]/[Cs] ratio, but also on a stage-dependent and Bi-dependent relative displacement of the intercalate and carbon π bands. The important point obtained from the foregoing discussion is that the number of holes per $CsBi_x$ formula unit is quite low. Specific-heat measurements should be carried out in these compounds to obtain further information regarding the $CsBi_x$ contribution to $D(E_F)$.

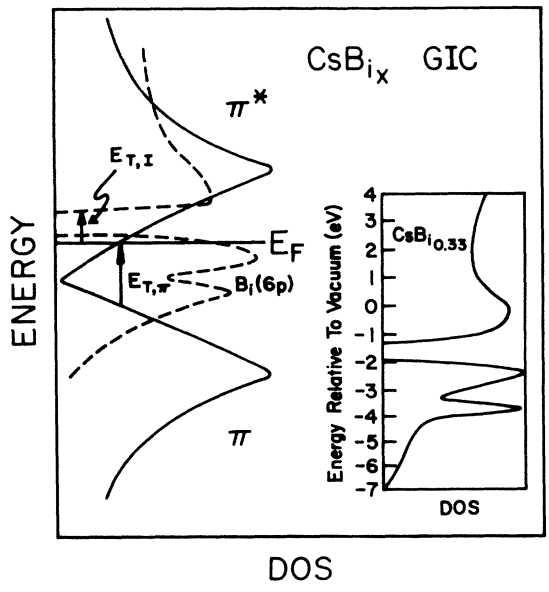

FIG. 4. Schematic density of states (DOS) for $CsBi_x$ GIC's. Carbon (π,π^*) states are designated by the solid lines, while the $CsBi_x$ states are designated by the dashed lines. The proposed $CsBi_x$ contribution to the DOS of the GIC is by analogy with that obtained from photoemission studies (Ref. 33) and optical absorption[39] of the $CsBi_{0.33}$ alloy, which is shown in the inset. A ~ 0.5-eV gap is shown for the $CsBi_x$ DOS, and the Fermi level is seen to cut through the carbon π^* bands and $CsBi_x$ valence bands, which have primarily Bi($6p$) character. The two vertical arrows labeled $E_{T,\pi}$ and $E_{T,I}$ indicate the carbon $\pi \rightarrow \pi^*$ and $CsBi_x$ interband transitions at the respective interband thresholds.

C. KHg GIC's

For the stage-1 and -2 KHg GIC's the Drude edges in $R(\omega)$ (Fig. 1) are located near 2.3 and 1.8 eV, respectively. The edges exhibit a very small shift relative to the value in the respective Hg-free binary GIC counterparts KC_8 (stage 1) and KC_{24} (stage 2). However, we ascribe no physical significance to this small shift. The positions of the Drude edges in KHg GIC's lie $\sim 0.8-1.3$ eV higher than in the corresponding-stage $CsBi_x$ GIC's. Several experimental[34–36] and theoretical[37,38] studies have found the charge transfer from the K($4s$) to the carbon π band is about 60–100% for KC_8 and $\sim 100\%$ for KC_{24}.

The addition of Hg to the K-intercalate layers in $KHgC_n$ ($n=4,8$) is also accompanied by a doubling ($n=4$) and tripling ($n=8$) of the [K]/[C] ratio over that in the binary corresponding-stage-index KC_8 and KC_{24} compounds, respectively. If, for the case of stage-1 compounds, one assumes for the moment complete charge transfer of K($4s$) electrons to the carbon π bands, and no charge transfer to the Hg-derived states, then the c-axis expansion accompanying the Hg uptake would be expected to lead to a decrease in ω_p. This follows from the BR model in which $\omega_{p,\pi}^2 \propto f_C/I_C$, and results in

$$\Delta\omega_{p,\pi}=\omega_p(KHgC_4)-\omega_p(KC_8)=-0.4 \text{ eV} ,$$

in contrast to the experimental observation $\Delta\omega_p^{\text{expt}}=+0.5$ eV. Thus one must conclude that there is a significant contribution to the effective plasma frequency from Hg-derived electrons. We apply the two-carrier model to qualitatively determine this contribution.

In Fig. 5, we show our schematic DOS model for KHg GIC's to qualitatively account for the optical data. The position of E_F is seen to intersect the π (solid line) and intercalate (dashed line) contributions to the total DOS. We show E_F intersecting the Hg($6s-6p$) band and not the K($4s$) band, but this decision is somewhat arbitrary. The π-band plasma frequency $\omega_{p,\pi}$, optical mass $m_{\text{opt},\pi}$, and charge transfer f_C are determined (as was done for $CsBi_x$ GIC's) via the identification of the midpoint of the $\pi\rightarrow\pi^*$ thresholds indicated by the arrows with error ±0.1 eV in Fig. 2(b): $E_{T,\pi}=3.2\pm0.1$ eV (stage 1) and $E_{T,\pi}=2.4\pm0.1$ eV (stage 2). The values for $E_F=E_{T,\pi}/2$, $\omega_{p,\pi}$, $m_{\text{opt},\pi}$, and f_C calculated from Eqs. (3)–(5) appear in Table I. Proceeding in the same way as for the $CsBi_x$ GIC's, we use Eq. (2) to find an experimental value for $\omega_{p,I}$. This procedure results in the values $\omega_{p,I}=4.12\pm0.03$ and 3.1 ± 0.05 eV for the stage-1 and -2 KHg GIC's, respectively, compared to the respective π-band contributions $\omega_{p,\pi}=3.0\pm0.05$ (stage 1) and 3.2 ± 0.1 eV (stage 2). Thus in the KHg GIC's we see that the π and intercalate contributions to ω_p are comparable, in sharp contrast to the $CsBi_x$ GIC's. In addition, we also find values for f_I of 1.78 (or 2.78) for stage 1, and 1.75 (or 2.75) for stage 2, if we choose two (or three) conduction electrons contributed per KHg unit. These two (three) electrons per KHg unit must supply both the π^* band(s) as well as the intercalate band(s). The large values for f_I obtained from ω_p and $E_{F,\pi}$ indicate that the majority of the available intercalate valence electrons remain as conduction electrons in the KHg-derived bands.

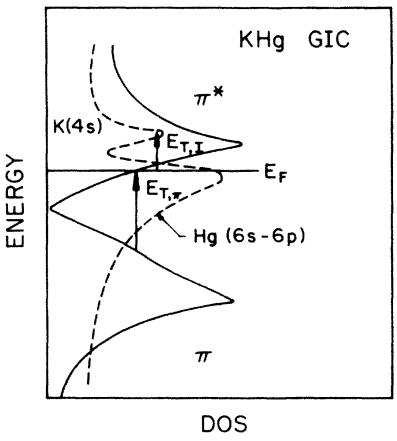

FIG. 5. Schematic density of states (DOS) of KHg GIC's. Carbon (π,π^*) and intercalant KHg states are shown as solid and dashed lines, respectively. The two vertical arrows correspond to optical transitions at the carbon inter-π-band threshold $E_{T,\pi}$ and a possible threshold $E_{T,I}$ for transitions between intercalate bands.

The interband dielectric function $\epsilon_{\text{inter},2}(\omega)$ of KHg GIC's (Fig. 2) also exhibits low-energy intercalate-derived structure. Besides the carbon $\pi\rightarrow\pi^*$ threshold (midpoint of the heavy line) indicated by the arrow, we observed the onset of interband absorption at 1.2 (stage 1) and 1.1 eV (stage 2), respectively. These onsets have also been identified previously with intercalate-derived transitions by Preil *et al.*[19] Based on the band structure of a single-layer 2×2 K-Hg-K superlattice reported by Senbetu *et al.*,[22] but using our significantly lower value for charge transfer (~0.2 electron per KHg unit), we place the Fermi level ~3 eV higher in their diagram. With E_F in this position the likely low-energy transitions are then between hybridized states involving Hg($6s$),($6p$), and K($4s$), which we show schematically in the DOS (Fig. 5). Clearly, a self-consistent energy-band calculation is needed to resolve this conjecture.

In contrast to the suggestion of localized Hg states near E_F in $KHgC_4$ proposed much earlier by Preil *et al.*[18] our analysis of the optical data requires a wide KHg-derived conduction band(s) to provide the necessary contribution $\omega_{p,I}$ to ω_p. These intercalant electrons may, in fact, be responsible for the superconducting properties of $KHgC_{4n}$ ($n=1,2$). As mentioned above, our present interpretation of the KHg-GIC optical data is also in sharp contrast with the placement of E_F by Senbetu *et al.* in their rigid-band model[22] for stage-2 $KHgC_8$, which leads to a large charge transfer (i.e., 1.5–2 electrons per KHg) to the carbon π band. We estimate that this charge transfer would result in a $\pi\rightarrow\pi^*$ threshold at ~4.6 eV (essentially at the M point). No threshold-type structure is observed in this energy range.

Intercalate-derived itinerant s character at E_F due to Hg($6s$) states is also consistent with the superconducting properties observed in KHg GIC's. From specific-heat measurements it has been determined[23] that the Fermi-surface density of states $N(E_F)$ is larger in stage-1 than in stage-2 GIC's. Our results find only a small, and probably insignificant, difference in the intercalate electron density between stage-1 and -2 KHg GIC's. This small difference suggests that the increase in the superconducting critical temperature T_c for the stage-2 over that of the stage-1 KHg GIC might be considered as being due to the differences in the intercalate electron-phonon interaction or the intercalate phonons themselves. However, valence band photoemission data by DiCenzo *et al.*[40] have been interpreted by them to indicate a higher occupancy of the Hg($6s$) states in stage-2 than in stage-1 $KHgC_n$.

IV. CONCLUSIONS

We have analyzed the optical dielectric function of the stage-1 and -2 $CsBi_x$ and KHg GIC's in terms of a schematic DOS model containing both graphitic π and intercalate contributions. The model is supported by optical data on both the free-carrier and interband components of $\epsilon(\omega)$.

The Fermi level is located experimentally in the graphitic carbon π^* band(s) via the identification of the interband $\pi\rightarrow\pi^*$ threshold structure in the $\epsilon_2(\omega)$ data.

This threshold energy $E_{T,\pi} \approx 2E_F$. Within the framework of the Blinowski-Rigaux rigid-band model for the carbon (π,π^*) bands we compute the π-electron plasma frequency $\omega_{p,\pi}$ from E_F, and the intercalate contribution $\omega_{p,I}$ from $\omega_{p,I}^2 = \omega_p^2 - \omega_{p,\pi}^2$. We assume an intercalate electron mass of $\sim 1\, m_e$ to obtain values for f_I—the intercalate free-carrier density. Of particular interest is that we found $f_I \sim 0.0$–0.11 for $CsBi_x$ GIC's, in sharp contrast to $f_I \sim 2$–3 for KHg GIC's, in units of holes/$CsBi_x$ or electrons/KHg. Thus in the case of $CsBi_x$ GIC's, the electrical transport properties are dominated by the light graphite π^* electrons, and the donated Cs($6s$) electrons remain in the intercalate layer, and nearly fill a lower lying B($6p$) band. The large value of f_I found for the KHg GIC's indicates that the transport properties of this GIC are strongly dependent on the intercalate-derived carriers.

In a comment to be published elsewhere,[13] using ac magnetic susceptibility, we found no evidence for superconductivity in the $CsBi_x$ GIC's. This finding is in disagreement with the previously published experimental results of Lagrange *et al.*[9] Our susceptibility experiments were carried out on samples with I_c values in good agreement with Lagrange *et al.*, and from the same sample preparations which yielded the optical samples studied in this work. The absence of superconductivity in our samples is consistent, however, with our observation that almost all electrons contributing to the plasma frequency are graphitic π electrons; i.e. there is little or no optical and susceptibility evidence for s character at the Fermi surface. In the KHg GIC's where superconductivity is well established, we find 2–3 electrons per KHg formula unit in intercalate states necessary to explain the high values of the experimental plasma frequency. These electrons are likely to occupy hybridized Hg($6s$-$6p$) states, and we suggest, as have DiCenzo *et al.*,[40] that these electrons are responsible for the superconductivity in the KHg GIC's.

ACKNOWLEDGMENTS

The authors are very grateful to Dr. A. W. Moore of Union Carbide for his generous gift of HOPG used in this study. The research at the University of Kentucky was supported by the U. S. Department of Energy under Grant No. DE-FG05-85ER45151.

[1] M. S. Dresselhaus and G. Dresselhaus, Adv. Phys. **30**, 139 (1981).
[2] S. A. Solin, Adv. Chem. Phys. **49**, 455 (1982).
[3] C. Rigaux, in *Intercalation in Layered Materials,* edited by M. S. Dresselhaus (Plenum, New York, 1987), p. 235.
[4] P. C. Eklund, M. H. Yang, and G. L. Doll, in *Intercalation in Layered Materials,* Ref. 3, p. 257.
[5] R. E. Heinz and P. C. Eklund, in *Intercalated Graphite,* edited by M. S. Dresselhaus, J. E. Fisher, and M. I. Moran (North-Holland, New York, 1983), p. 81.
[6] G. L. Doll, M. H. Yang, and P. C. Eklund, Phys. Rev. B **35**, 9790 (1987).
[7] P. Lagrange, M. El Makrini, D. Guérard, and A. Hérold, Physica **99B**, 473 (1980).
[8] M. H. Yang, P. C. Eklund, and W. A. Kamitakahara, in *Graphite Intercalation Compounds,* Extended Abstracts, edited by P. C. Eklund, M. S. Dresselhaus, and G. Dresselhaus (Materials Research Society, Pittsburgh, 1984), p. 127.
[9] P. Lagrange, A. Bendriss-Rerhrhaye, J. F. Mareche, and E. McRae, Synth. Met. **12**, 201 (1985).
[10] M. H. Yang, and P. C. Eklund, J. Mater. Res. **1**, 827 (1987).
[11] M. G. Alexander, D. P. Goshorn, D. Guérard, P. Lagrange, M. El Makrini, and D. G. Onn, Synth. Met. **2**, 203 (1980).
[12] Y. Iye and S. Tanuma, Phys. Rev. B **25**, 4583 (1982).
[13] M. H. Yang, P. C. Eklund, and L. E. Delong (unpublished).
[14] Y. Koike and S. Tanuma, J. Phys. Soc. Jpn. **50**, 1964 (1981).
[15] L. A. Pendrys, R. A. Wachnik, and F. L. Vogel, Synth. Met. **5**, 277 (1983).
[16] L. E. Delong, P. C. Eklund, V. Tondiglio, S. E. Lambert, and M. B. Maple, Phys. Rev. B **26**, 6315 (1982); L. E. Delong and P. C. Eklund, Synth. Met. **5**, 291 (1983).
[17] Y. Iye and S. Tanuma, Synth. Met. **5**, 257 (1983).
[18] M. E. Preil and J. E. Fischer, Synth. Met. **8**, 149 (1983).
[19] M. E. Preil, L. A. Grunes, J. J. Ritsko, and J. E. Fischer, Phys. Rev. B **30**, 5852 (1984).
[20] M. E. Preil and J. E. Fischer, Synth. Met. **8**, 149 (1983).
[21] J. E. Fischer, J. M. Bloch, C. C. Shieh, M. E. Preil, and K. Jelley, Phys. Rev. B **31**, 4773 (1985).
[22] L. Senbetu, H. Ikezi, and C. Umrigar, Phys. Rev. B **32**, 750 (1985).
[23] M. G. Alexander, D. P. Goshorn, D. Guérard, P. Lagrange, M. El Makrini, and D. G. Onn, Solid State Commun. **38**, 103 (1981).
[24] F. Wooten, *Optical Properties of Solids* (Academic, New York, 1972), p. 248.
[25] D. M. Hoffman, H. R. Heinz, G. L. Doll, and P. C. Eklund, Phys. Rev. B **32**, 1278 (1985).
[26] E. A. Taft and H. R. Philipp, Phys. Rev. **138**, A197 (1965).
[27] J. Blinowski, N. H. Hau, C. Rigaux, J. P. Vieren, R. LeToullec, G. Furdin, A. Hérold, and J. Melin, J. Phys. (Paris) **41**, 47 (1980).
[28] J. Zhang, D. M. Hoffman, and P. C. Eklund, Phys. Rev. B **34**, 4316 (1986).
[29] G. Guérard, G. M. T. Foley, M. Zanini, and J. E. Fischer, Il Nuovo Cimento, **38B**, 41 (1977).
[30] P. Pfluger, P. Oelhafen, H. U. Künzi, R. Jeker, E. Hauser, K. P. Ackermann, M. Müller, and H.-J. Güntherodt, Physica **99B**, 395 (1980).
[31] K.W.-K. Shung, Phys. Rev. B **34**, 1264 (1986).
[32] W. E. Spicer, Phys. Rev. Lett. **11**, 243 (1963).
[33] F. Wooten, J. P. Hernandez, and W. E. Spicer, J. Appl. Phys. **44**, 1112 (1973).
[34] J. J. Ritsko, Phys. Rev. B **25**, 6452 (1982).
[35] M. E. Preil and J. E. Fischer, Phys. Rev. Lett. **52**, 1141 (1984).
[36] T. Takahashi, N. Gunasekara, T. Sagawa, and H. Suematsu, in *Graphite Intercalation Compounds,* Extended Abstracts, edited by M. S. Dresselhaus, G. Dresselhaus, and S. A. Solin (Materials Research Society, Pittsburgh, 1986), p. 77.
[37] T. Ohno, K. Nakao, and H. Kamimura, J. Phys. Soc. Jpn. **47**, 1125 (1979).
[38] D. P. DiVincenzo and S. Rabii, Phys. Rev. B **25**, 4110 (1982).
[39] A. H. Sommer and W. E. Spicer, J. Appl. Phys. **32**, 1036 (1961).
[40] S. B. DiCenzo, P. A. Rosenthal, H. J. Kim, and J. E. Fischer, Phys. Rev. B **34**, 3620 (1986).